Engineering Science and Technology, an International Journal xxx (2016) xxx–xxx

HOSTED BY

ELSEVIER

Contents lists available at ScienceDirect

Engineering Science and Technology, an International Journal

journal homepage: www.elsevier.com/locate/jestch

Full Length Article

Mathematical modelling of nonlinear thermal radiation effects on EMHD peristaltic pumping of viscoelastic dusty fluid through a porous medium duct

M.M. Bhatti [a], A. Zeeshan [b,*], N. Ijaz [b], O. Anwar Bég [c], A. Kadir [d]

[a] Shanghai Institute of Applied Mathematics and Mechanics, Shanghai University, Shanghai, China
[b] Department of Mathematics and Statistics, International Islamic University, Islamabad, Pakistan
[c] Aeronautical & Mechanical Engineering Department, University of Salford, Manchester M54WT, UK
[d] Spray Research Group, Petroleum and Gas Engineering, School of Computing, Science and Engineering, Newton Building, University of Salford, Manchester M54WT, UK

ARTICLE INFO

Article history:
Received 24 August 2016
Revised 27 October 2016
Accepted 7 November 2016
Available online xxxx

Keywords:
Heat transfer
Thermal radiation
Solid particle
Dusty fluid
Electromagnetohydrodynamics
Peristaltic propulsion
Particle volume fraction

ABSTRACT

Biologically-inspired propulsion systems are currently receiving significant interest in the aerospace sector. Since many spacecraft propulsion systems operate at high temperatures, thermal radiation is important as a mode of heat transfer. Motivated by these developments, in the present article, the influence of nonlinear thermal radiation (via the Rosseland diffusion flux model) has been studied on the laminar, incompressible, dissipative EMHD (Electro-magneto-hydrodynamic) peristaltic propulsive flow of a non-Newtonian (Jefferys viscoelastic) dusty fluid containing solid particles through a porous planar channel. The fluid is electrically-conducting and a constant static magnetic field is applied transverse to the flow direction (channel walls). Slip effects are also included. Magnetic induction effects are neglected. The mathematical formulation is based on continuity, momentum and energy equations with appropriate boundary conditions, which are simplified by neglecting the inertial forces and taking the long wavelength and lubrication approximations. The boundary value problem is then rendered non-dimensional with appropriate variables and the resulting system of *reduced ordinary differential equations* is solved analytically. The impact of various emerging parameters dictating the non-Newtonian propulsive flow i.e. *Prandtl number, radiation parameter*, *Hartmann number*, *permeability parameter*, *Eckert number*, *particle volume fraction*, *electric field and slip parameter* are depicted graphically. Increasing particle volume fraction is observed to suppress temperature magnitudes. Furthermore the computations demonstrate that an increase in particle volume fraction reduces the pumping rate in retrograde pumping region whereas it causes the opposite effect in the co-pumping region. The trapping mechanism is also visualized with the aid of streamline contour plots. Increasing thermal radiation elevates temperatures. Increasing Hartmann (magnetic body force) number decreases the size of the trapping bolus whereas the quantity of the does not effected. Conversely increasing particle volume fraction reduces the magnitude of the trapping bolus whereas the number of trapped bolus remains constant.

1. Introduction

Thermal radiation heat transfer is known to have an important influence on many industrial processes and technological devices at high temperature. These include rocket propulsion [1], plume dynamics [2], solar collector performance [3], materials processing [4], combustion systems [5] and fire propagation [6]. With developments in computational and analytical tools, in recent years, increasing attention has been directed at thermal convection flows with significant radiative flux. In various convection and conduction problems the rate of energy transfer between two points is strongly dependent on the temperature difference at the locations of order one. However, the transfer rate of energy due to thermal radiation between two bodies is dependent upon the absolute temperature difference. It is well established that the importance of radiation is intensified when the absolute temperature is very high. In particular thermal boundary layer flows with strong radiation have stimulated substantial interest. The integro-differential nature of the governing equation of radiative heat transfer makes even numerical solutions of coupled radiative-convective flows

* Corresponding author.
E-mail address: ahmad.zeeshan@iiu.edu.pk (A. Zeeshan).
Peer review under responsibility of Karabuk University.

http://dx.doi.org/10.1016/j.jestch.2016.11.003
2215-0986/

Nomenclature

$\tilde{U}, \tilde{V}$	velocity components (m/s)
$\tilde{X}, \tilde{Y}$	Cartesian coordinates (m)
C	volume fraction density
$\tilde{P}$	pressure in fixed frame (N/m^2)
k	permeability (m^2)
$\tilde{a}$	wave amplitude (m)
$\tilde{b}$	width of the channel (m)
$\tilde{c}$	wave velocity (m/s)
E_c	Eckert number
P_r	Prandtl number
Re	Reynolds number
$\tilde{t}$	time (s)
c	effective heat capacity (J/K)
$\boldsymbol{B}$	magnetic field (T)
$\bar{k}$	mean absorption coefficient
S	drag force
k	thermal conductivity
R_d	radiation-conduction parameter
T	temperature (K)
$\boldsymbol{E}$	electric field (V/m)
$\tilde{\boldsymbol{V}}$	velocity field (m/s)
Q	volume flow rate (m^3/s)
$\boldsymbol{S}$	stress tensor
$\boldsymbol{J}$	current density (A)

Greek symbols

θ	dimensionless temperature
λ	wavelength (m)
μ_s	viscosity of dusty viscoelastic fluid (Ns/m^2)
ϕ	amplitude ratio
σ	electrical conductivity of dusty viscoelastic fluid (S/m)
$\bar{\sigma}$	Stefan-Boltzmann constant
ϖ_T	Thermal equilibrium time
ϖ_v	relaxation time of the particle
β	slip parameter
ρ	fluid density (kg/m^3)
λ_1	relaxation time
λ_2	retardation time
γ	shear rate
φ	stream function

Subscripts

f	fluid phase
p	particulate phase

challenging. Recourse is therefore generally made to one of the many algebraic flux models developed which are differential in nature and while simplifying the mathematical complexity retain important physical characteristics of actual radiative transfer processes. Examples of such models include the Milne-Eddington approximation [7], Rosseland diffusion flux model [8], Schuster-Schwartzchild two-flux model [9], Traugott P1 differential model [10] and the Cogley-Vincenti-Giles flux model [11]. An excellent summary of these and other models is provided by Siegel and Howell [12]. Numerous studies have employed such models to investigate heat and also mass transfer in boundary layer and fully-developed laminar convection flows. These studies have explored numerous simultaneous *multi-physical* effects in addition to radiative heat transfer including magnetic nanofluid flow [13], gravity and pressure gradient effects [14], buoyancy effects [15], unsteady stretching surface flow [16], ferrofluid dynamics [17], time-dependent, wall injection and Soret/Dufour effects [18]. These studies have however been confined to *Newtonian* flows. Recent developments in novel propellants for spacecraft [19] have identified the significant potential of non-Newtonian flows in ducts with radiative transfer. These developments are on ongoing and have diversified the application of non-Newtonian fluid models, in particular viscoelastic theories (e.g. second order Reiner-Rivlin model [20]) to a new branch of propulsion studies including droplet atomization, thermal relaxation and radiating reactive phenomena. The constitutive equations for many such fluids are elaborated in detail by Irgens [21]. Furthermore in the process chemical industry, radiative flows of non-Newtonian fluids are also of great interest in high temperature fabrication of polymers and plastics. Most studies in this regard have employed the Rosseland model which is generally valid for optically-thick boundary layers. Recently Gaffar et al. [22] used the Jeffreys viscoelastic model and a finite difference to study enrobing flow and high temperature heat transfer from a circular cylindrical body. Abdel and Masheha [23] used a perturbation technique to derive solutions for the influence of Chandrsekhar (magnetic) number on magneto-hydrodynamic boundary layer flow and heat transfer of a Walter's liquid B viscoelastic from a stretching sheet with radiative flux and non-uniform heat source. Gupta et al. [24] applied a finite element method and the Eringen micro-structural model to simulate mixed convective flow from a shrinking polymer sheet under strong radiative heat flux. Khan et al. [25] studied radiative convection stagnation-point flow of a Sisko viscoelastic fluid from a stretching cylinder obtaining numerical solutions with the fourth order Runge-Kutta method and a shooting technique. Uddin et al. [25] used Maple numerical quadrature and Lie group algebra to investigate radiation effects on power-law nanofluid flow in high permeability media. Mustafa et al. [27] used the Maxwell elasto-viscous model to analyze rotating non-Newtonian thermal convection flow from an exponentially stretching impermeable surface with strong radiative heat transfer. Subba Rao et al. [28] used Keller's box method to derive computational solutions for radiation flux effects on Casson viscoplastic boundary layer slip flow in a complex porous medium.

In the above studies, generally, the channel walls or boundary (ies) were assumed to be *rigid*. Peristaltic pumping is an important biological mechanism which is generated by the symmetrical contraction and expansion of a *flexible boundary* e.g. flow in the human digestive tract. Propulsion due to peristaltic wave motion is also encountered in other physiological and zoological phenomena including transport of blood in cardiac chambers, embryological transport, earthworm and snake locomotion. An excellent summary of the fluid mechanics of peristalsis has been provided by Fung [29]. In recent years, many other engineering disciplines have embraced the bio-inspiration of peristalsis to improve existing designs. In the context of biomimetic pumping systems for spacecraft systems, important progress was made at Caltech's Jet Propulsion Laboratory (JPL) in the 1990 s, as elaborated by Bar-Cohen and Chatig [30]. Further developments in bio-inspired peristaltic pumps for chemical and nuclear engineering waste transport (which avoid the inherent problems of conventional pumping systems e.g. leakage, backflow etc) have been reported by Shkolnikov et al. [31]. Magnetohydrodynamic (MHD) peristaltic propulsion in which fluids are electrically-conducting and can be manipulated by externally applied magnetic fields (radially or axially) has also stimulated substantial interest in space propulsion. Slough et al. [32] describe important progress in this regard peristaltic, pulsed inductive acceleration of non-ferritic particles for space propul-

Please cite this article in press as: M.M. Bhatti et al., Mathematical modelling of nonlinear thermal radiation effects on EMHD peristaltic pumping of viscoelastic dusty fluid through a porous medium duct, Eng. Sci. Tech., Int. J. (2016), http://dx.doi.org/10.1016/j.jestch.2016.11.003

sion. In this so-called Macron Launched Propulsion (MLP) system, fluids can be electromagnetically controlled for micro-scale and nano-scale operations on space stations. Other important applications of magnetized peristaltic flows in biochemical engineering have been identified by Kim et al. [33] who have also computed efficient operating frequencies and described robust microfabrication methods. These technological strides have stimulated considerable interest in the refinement of mathematical models of *magnetic peristaltic propulsion* in both purely fluid and also saturated porous media. Many multi-physical simulations with and without convective and/or radiative heat transfer have been communicated. Representative studies in this regard include Hayat et al. [34] who also considered convective heat transfer in peristaltic wave propagation in conduits. Tripathi and Bég [35] addressed transient and finite length effects in hydromagnetic peristaltic pump flows. Srinivas and Kothandapani [36] studied combined heat and species diffusion in magnetic peristaltic flow in porous media with wall deformation. Several authors have also examined non-Newtonian magnetohydrodynamic peristaltic propulsion. Pandey and Chaube [37] obtained analytical solutions for peristaltic pumping of magnetized Eringen micropolar lqiuids in tubes. Bég et al. [38] used the Williamson viscoelastic model to theoretically hydromagnetic peristaltic pumping in conduits and obtained semi-numerical solutions with a modified Zhou differential transform method (DTM). Further studies of non-Newtonian MHD peristaltic pumping have been communicated recently by Hayat et al. [39] and Akbar et al. [40]. In the context of porous media peristaltic flows, several excellent studies have also been communicated. Porous media provide a robust mechanism for regulating flows and damping. A porous medium comprises a solid matrix (either rigid or deformable) which is interconnected with voids which are in single phase systems, saturated with the percolating fluid. The flow quantities such as velocity, pressure are generally irregular on the microscopic scale and the Darcy law (or modifications) is valid for low Reynolds, viscous-dominated flows, which characterize peristaltic systems. Recent studies in this regard include Khan et al. [41] who deployed the third grade differential viscoelastic model and Tripathi et al. [42] who studied peristaltic pumping of a fractional Oldroyd-B viscoelastic fluid in Darcy-Brinkman porous media. These studies showed that trapping and axial velocities are strongly influenced by permeability of the porous medium. Radiative heat transfer effects on peristaltic flow of Sikso viscoelastic fluids has also been studied by Mehmood and Fetecau [43], wherein it has been shown that temperatures are elevated with increasing radiation parameter, amplitude ratio, and channel width ratio.

The above investigations have invariably considered *single-phase* systems. However in many technological applications including micro-propulsion, vapour deposition, combustion, aerosol filtration and lunar ash flow, multi-phase suspensions arise. Such systems are often referred to as "dusty" fluids and the solid particle motion in these fluid-particulate suspensions has a significant influence on thermofluid characteristics. Thermal conductivity of working fluids in industrial devices may be improved via the careful introduction of small solid particles in the fluids to form slurries. These particles may be polymeric, metallic or non-metallic. The thermal conductivity of dusty fluids i.e. fluids with suspended solid particles can be manipulated to be greater than conventional fluids. Magnetohydrodynamic dusty flows are also of relevance to magnetic propulsion systems, accelerators, plasma energy generators etc. The performance and efficiency of these devices are affected by the presence of solid particles that may be present in the form of soot or ash. When the particle concentration is very high, this may manifest in mutual particle interaction with higher phase viscous stresses and can result in a particle phase viscosity. Marble [44] has provided a lucid summary of dusty fluid mechanics and transport phenomena. Several analyses of peristaltic flows of dusty fluids have been reported in the scientific literature. Mekheimer et al. [45] obtained perturbation solutions for peristaltic hydrodynamics of a particle fluid suspension in a planar channel, discussing the influence of particle concentration on augmented and other pumping modes. Bhatti and Zeeshan [46] obtained closed-form solutions for slip peristaltic flow of viscoplastic Casson fluid-particle suspension in a channel. They showed that increasing particle volume fraction decelerates the flow along the channel. Nagarani and Sarojamm [47] derived perturbation solutions for peristaltic transport of power law fluids containing a suspension of small particles in a two-dimensional channel, noting that velocity of the suspended particles is markedly lower than that of the fluid under various pumping conditions. Kamel et al. [48] studied slip effects on peristaltic propulsion of fluid-particle suspensions, observing that critical reflux pressure is of lesser magnitude for the particle–fluid suspension compared with the particle-free fluid and is sensitive to wall slip.

With recent developments in high-temperature peristaltic pumping in mind and also novel particulate non-Newtonian propellants [49], the current study examines theoretically *nonlinear thermal radiation effects on EMHD peristaltic propulsion of non-Newtonian fluid-particle (dusty) suspensions in a planar channel containing a homogenous porous medium*. Both electrical and magnetic field effects are considered for the first time in dusty peristalstic dynamics. The Jeffreys viscoelastic model is employed to mimic rheological properties since this model has not been explored extensively in dusty fluid dynamics although it provides a good representation for propellants. The governing equations for fluid phase and particle phase are modeled by neglecting the inertial forces and considered the long wave length approximation. The transformed, non-dimensional coupled differential equations of momentum and energy for both particulate and fluid phases are solved analytically under physically realistic boundary conditions. The influence of emerging parameters on velocity, temperature and pressure rise distributions is elaborated at length. Furthermore contour plots for streamlines are provided to visualize trapping phenomena and sensitivity to non-Newtonian and other parameters. The current mathematical problem, to the authors' knowledge, has not been investigated in the technical literature.

2. Mathematical model

Consider the peristaltic flow and heat transfer in a dusty Jeffrey's viscoelastic fluid-particle suspension induced by sinusoidal wave motion of walls in a two-dimensional planar channel containing an isotropic, homogenous porous medium. Temperature is sufficiently high to invoke nonlinear thermal radiation effects. Thermal radiation is assumed to be present in the form of a unidirectional flux in the $\tilde{Y}$ – direction i.e. q_r. Viscous heating and heat generation/absorption effects are present. The fluid-suspension is electrically-conducting, gray, emitting and absorbing, but *non-scattering* and the flow is subjected to a transverse constant magnetic field of strength, B_o. Magnetic induction and Hall current effects are neglected. A Cartesian coordinate system is selected i.e. the $\tilde{X}$-axis is orientated along the *longitudinal axis* of the channel i.e. in the direction of wave propagation while the $\tilde{Y}$-axis is taken normal to it. The physical model is illustrated in Fig. 1.

The geometry of the wall can be written as:

$$\tilde{H}(\tilde{X},\tilde{t}) = \tilde{a} + \tilde{b}\sin\frac{2\pi}{\lambda}(\tilde{X} - \tilde{c}\tilde{t}). \tag{1}$$

The magnetic field is considered of the following form:

$$\boldsymbol{B} = (0, B_0), \tag{2}$$

Please cite this article in press as: M.M. Bhatti et al., Mathematical modelling of nonlinear thermal radiation effects on EMHD peristaltic pumping of viscoelastic dusty fluid through a porous medium duct, Eng. Sci. Tech., Int. J. (2016), http://dx.doi.org/10.1016/j.jestch.2016.11.003

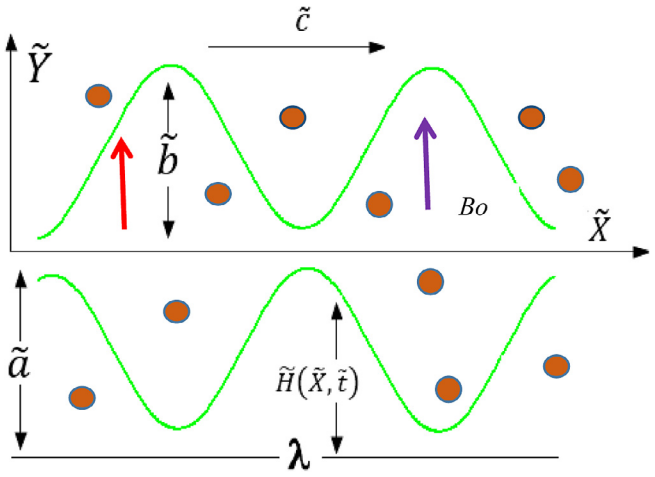

Fig. 1. Geometry of MHD non-Newtonian dusty peristaltic propulsion in a porous medium channel.

Ohm's Law states:

$$\boldsymbol{J} = \sigma[\boldsymbol{E} + \tilde{\boldsymbol{V}} \times \boldsymbol{B}]. \tag{3}$$

The governing equation of continuity, linear momentum and energy equations for fluid phase and dust phase (incorporating the appropriate Lorentzian magnetohydrodynamic body force terms only in the fluid phase) can be written, following Mekheimer et al. [45], Bhatti and Zeshan [46], Nagarani and Sarojamm [47] and Kamel et al. [48], as:

Fluid phase:

$$\frac{\partial \tilde{U}_f}{\partial \tilde{X}} + \frac{\partial \tilde{V}_f}{\partial \tilde{Y}} = 0, \tag{4}$$

$$(1-C)\rho_f\left(\frac{\partial \tilde{U}_f}{\partial \tilde{t}} + \tilde{U}_f\frac{\partial \tilde{U}_f}{\partial \tilde{X}} + \tilde{V}_f\frac{\partial \tilde{U}_f}{\partial \tilde{Y}}\right) = -(1-C)\frac{\partial \tilde{P}}{\partial \tilde{X}} + (1-C)\left(\frac{\partial}{\partial \tilde{X}}S_{\tilde{X}\tilde{X}} + \frac{\partial}{\partial \tilde{Y}}S_{\tilde{X}\tilde{Y}}\right) + \frac{CS}{\varpi_v}\left(\tilde{U}_p - \tilde{U}_f\right) + J_{\tilde{X}} \times B - \frac{\mu_s}{K}\tilde{U} \tag{5}$$

$$(1-C)\rho_f\left(\frac{\partial \tilde{V}_f}{\partial \tilde{t}} + \tilde{U}_f\frac{\partial \tilde{V}_f}{\partial \tilde{X}} + \tilde{V}_f\frac{\partial \tilde{V}_f}{\partial \tilde{Y}}\right) = -(1-C)\frac{\partial \tilde{P}}{\partial \tilde{Y}} + (1-C)\left(\frac{\partial}{\partial \tilde{X}}S_{\tilde{Y}\tilde{X}} + \frac{\partial}{\partial \tilde{Y}}S_{\tilde{Y}\tilde{Y}}\right) + \frac{CS}{\varpi_v}(\tilde{V}_p - \tilde{V}_f) + J_{\tilde{Y}} \times B - \frac{\mu_s}{K}\tilde{V}, \tag{6}$$

$$(1-C)\rho_f c\left(\frac{\partial T_f}{\partial \tilde{t}} + \tilde{U}_f\frac{\partial T_f}{\partial \tilde{X}} + \tilde{V}_f\frac{\partial T_f}{\partial \tilde{Y}}\right) = \mathrm{k}(1-C)\frac{\partial^2 T_f}{\partial \tilde{Y}^2} + \frac{\rho_p c_p C}{\varpi_T}(T_p - T_f) + \frac{CS}{\varpi_v}(\tilde{U}_f - \tilde{U}_p)^2 + \frac{\partial \tilde{U}_f}{\partial \tilde{Y}}(1-C)S_{\tilde{X}\tilde{Y}} - \frac{\partial q_r}{\partial \tilde{Y}} + \sigma(E - B_0\tilde{U}_f)^2, \tag{7}$$

Dust phase:

$$\frac{\partial \tilde{U}_p}{\partial \tilde{X}} + \frac{\partial \tilde{V}_p}{\partial \tilde{Y}} = 0, \tag{8}$$

$$C\rho_p\left(\frac{\partial \tilde{U}_p}{\partial \tilde{t}} + \tilde{U}_p\frac{\partial \tilde{U}_p}{\partial \tilde{X}} + \tilde{V}_p\frac{\partial \tilde{U}_p}{\partial \tilde{Y}}\right) = -C\frac{\partial \tilde{P}}{\partial \tilde{X}} + \frac{CS}{\varpi_v}(\tilde{U}_f - \tilde{U}_p), \tag{9}$$

$$C\rho_p\left(\frac{\partial \tilde{V}_p}{\partial \tilde{t}} + \tilde{U}_p\frac{\partial \tilde{V}_p}{\partial \tilde{X}} + \tilde{V}_p\frac{\partial \tilde{V}_p}{\partial \tilde{Y}}\right) = -C\frac{\partial \tilde{P}}{\partial \tilde{Y}} + \frac{CS}{\varpi_v}(\tilde{V}_f - \tilde{V}_p), \tag{10}$$

$$\rho_p Cc\left(\frac{\partial T_p}{\partial \tilde{t}} + \tilde{U}_p\frac{\partial T_p}{\partial \tilde{X}} + \tilde{V}_p\frac{\partial T_p}{\partial \tilde{Y}}\right) = \frac{\rho_p Cc}{\varpi_T}(T_f - T_p), \tag{11}$$

The mathematical expression for the drag coefficient and the empirical relation for the viscosity of the fluid-particle (dusty) suspension can be defined [46–48] as follows:

$$S = \frac{9\mu_0}{2\tilde{a}^2}\tilde{\lambda}(C), \quad \tilde{\lambda}(C) = \frac{4 + 3\sqrt{8C - 3C^2} + 3C}{(2-3C)^2},$$
$$\mu_s = \frac{\mu_0}{1-\chi C}, \quad \chi = 0.07e^{[2.49C + \frac{1107}{T}e^{-1.69C}]}. \tag{12}$$

Employing a Rosseland diffusion flux model, the integro-differential equation for radiative transfer can be reduced to a Fourier-type diffusion equation analogous to that describing heat conduction, groundwater flow, electrostatic potential etc. It is important to note that the Rosseland model is quite accurate for optically-thick media where thermal radiation propagates a limited distance prior to encountering scattering or absorption. The refractive index of the fluid-particle suspension is assumed to be constant, intensity within the fluid is nearly isotropic and uniform and wavelength regions exist where the optical thickness is usually in excess of five [24,26]. The nonlinear radiative heat flux can be written effectively as:

$$q_r = -\frac{4\bar{\sigma}}{3\bar{k}}\frac{\partial T^4}{\partial \tilde{Y}} = -\frac{16\bar{\sigma}T^3}{3\bar{k}}\frac{\partial T}{\partial \tilde{Y}}. \tag{13}$$

The dusty fluid has viscoelastic characteristics and to this end the Jeffreys model is implemented. The appropriate stress tensor is:

$$\mathbf{S} = \frac{\mu_s}{1+\lambda_1}(\dot{\gamma} + \lambda_2\ddot{\gamma}). \tag{14}$$

To simplify the peristaltic flow problem it is convenient to describe the transformation of variables from the *fixed frame* to the *wave (laboratory) frame*:

$$\tilde{X} = \tilde{X} - \tilde{c}\tilde{t}, \quad \tilde{Y} = \tilde{Y}, \quad \tilde{U}_{f,p} = \tilde{U}_{f,p} - \tilde{c}, \quad \tilde{V}_{f,p} = \tilde{V}_{f,p}, \quad \tilde{P} = \tilde{P}. \tag{15}$$

The *moving boundary value problem* may be further simplified by the introduction of the following non-dimensional quantities

$$x = \frac{\tilde{X}}{\tilde{\lambda}}, \quad y = \frac{\tilde{Y}}{\tilde{a}}, \quad u_{f,p} = \frac{\tilde{U}_{f,p}}{\tilde{c}}, \quad v_{f,p} = \frac{\tilde{V}_{f,p}}{\tilde{c}\delta}, \quad h = \frac{\tilde{H}}{\tilde{a}}, \quad \phi = \frac{\tilde{b}}{\tilde{a}},$$
$$p = \frac{\tilde{a}^2}{\tilde{\lambda}\tilde{c}\mu_s}\tilde{P}, \quad \mathrm{Re} = \frac{\rho\tilde{a}\tilde{c}}{\mu_s}, \quad \theta_{f,p} = \frac{T_{f,p} - T_0}{T_1 - T_0}, \quad P_r = \frac{\mu_s c}{k},$$
$$\mathrm{E_c} = \frac{\tilde{c}^2}{c(T_1 - T_0)}, \quad N = \frac{S\tilde{a}^2}{\varpi_v\mu_s}, \quad R_d = \frac{4\bar{\sigma}T^3}{\mu_s c\bar{k}}, \quad k = \frac{K}{b_0},$$
$$\Gamma_1 = \frac{\sigma}{(1-C)c(T_1 - T_0)}, \quad \Gamma_2 = \frac{2B_0 Ec}{(1-C)c(T_1 - T_0)}. \tag{16}$$

Using Eqs. (15) and (16) in Eqs. (4)–(11), and taking the long wavelength and low Reynolds number approximations (i.e. lubrication theory), the resulting equations for the *fluid phase* can be written as follows:

$$\frac{1}{1-C}\frac{dp}{dx} = \frac{1}{1+\lambda_1}\frac{\partial^2 u_f}{\partial y^2} - \left(M^2 + \frac{1}{k}\right)(u_f + 1) + E, \tag{17}$$

$$\left(\frac{1}{\mathrm{P_r}} + \frac{4}{3}R_d\right)\frac{\partial^2 \theta_f}{\partial y^2} + \frac{E_c}{1+\lambda_1}\left(\frac{\partial u_f}{\partial y}\right)^2 + \frac{E_c}{N_1(1-C)}\left(\frac{dp}{dx}\right)^2 + M^2(u_f + 1)^2 E_c - \Gamma_2(u_f + 1) + \Gamma_1 = 0, \tag{18}$$

Please cite this article in press as: M.M. Bhatti et al., Mathematical modelling of nonlinear thermal radiation effects on EMHD peristaltic pumping of viscoelastic dusty fluid through a porous medium duct, Eng. Sci. Tech., Int. J. (2016), http://dx.doi.org/10.1016/j.jestch.2016.11.003

The equations for the *particulate phase* emerge as:

$$u_p = u_f - \frac{dp}{dx}\frac{1}{N} \tag{19}$$

$$\theta_p = \theta_f. \tag{20}$$

The corresponding non-dimensional boundary conditions are found to be:

$$u_f'(0) = 0, \quad \theta_f(0) = 0 \text{ and } u_f(h) = -1 - \frac{\beta}{1+\lambda_1}u_f'(h),$$
$$\theta_f(h) = 1, \quad h = 1 + \phi \sin 2\pi x. \tag{21}$$

The parameter N featured in Eqs. (22) and (23) is defined as:

$$\boldsymbol{N} = \sqrt{\boldsymbol{M}^2 + \frac{1}{\boldsymbol{k}}}. \tag{31}$$

The *volumetric flow rate* is given by integrating across the channel span:

$$Q = (1-C)\int_0^h u_f \mathrm{d}y + C\int_0^h u_p \mathrm{d}y. \tag{32}$$

The pressure gradient dp/dx is obtained after solving Eq. (32) and takes the form:

$$\frac{dp}{dx} = -\frac{(-1+C)N_1(\sqrt{1+\lambda_1}N(-Eh+N^2(h+Q))\cosh\sqrt{1+\lambda_1}Nh + (E-EhN^2\beta+N^4(h+Q)\beta)\sinh\sqrt{1+\lambda_1}hN)}{h\sqrt{1+\lambda_1}N((-1+C)CN^2-N_1)\cosh\sqrt{1+\lambda_1}Nh + (N_1+(-1+C)ChN^4\beta - hN^2N_1\beta)\sinh\sqrt{1+\lambda_1}hN}. \tag{33}$$

3. Analytical solutions

The linearization of the boundary value problem permits the extraction of closed-form solutions. The exact solution of Eqs. (17)–(20) may be shown to take the form:

$$u_f = c_3 + c_4\cosh\sqrt{1+\lambda_1}Ny, \tag{22}$$

$$u_p = c_3 + c_4\cosh\sqrt{1+\lambda_1}Ny - \frac{dp}{dx}\frac{1}{N_1}, \tag{23}$$

$$\theta_{f,p} = c_5 y + c_6 y^2. \tag{24}$$

The constants $C_i (i = 1, 2, 3\ldots)$ appearing in the above equations are defined as follows:

$$\boldsymbol{c_1} = -\frac{(\boldsymbol{1}+\boldsymbol{\lambda_1})((-\boldsymbol{1}+\boldsymbol{C})\boldsymbol{E}+\frac{\boldsymbol{dp}}{\boldsymbol{dx}})}{(-\boldsymbol{1}+\boldsymbol{C})\boldsymbol{N}(\sqrt{\boldsymbol{1}+\boldsymbol{\lambda_1}}\cosh\sqrt{\boldsymbol{1}+\boldsymbol{\lambda_1}}\boldsymbol{Nh}+\boldsymbol{N}\beta\sinh\sqrt{\boldsymbol{1}+\boldsymbol{\lambda_1}}\boldsymbol{hN})}, \tag{25}$$

$$\boldsymbol{c_2} = \frac{\boldsymbol{P_r}}{\boldsymbol{1}+\frac{\boldsymbol{4}}{\boldsymbol{3}}\boldsymbol{P_r}\boldsymbol{R_d}}, \tag{26}$$

$$\boldsymbol{c_3} = \frac{\sqrt{\boldsymbol{1}+\boldsymbol{\lambda_1}}\left((-\boldsymbol{1}+\boldsymbol{C})\left(\boldsymbol{E}-\boldsymbol{N^2}\right)+\frac{\boldsymbol{dp}}{\boldsymbol{dx}}\right)\cosh\sqrt{\boldsymbol{1}+\boldsymbol{\lambda_1}}\boldsymbol{Nh}+\boldsymbol{N}\left((-\boldsymbol{1}+\boldsymbol{C})(\boldsymbol{E}-\boldsymbol{N^2})+\frac{\boldsymbol{dp}}{\boldsymbol{dx}}\right)\boldsymbol{\beta}\sinh\sqrt{\boldsymbol{1}+\boldsymbol{\lambda_1}}\boldsymbol{hN}}{(-\boldsymbol{1}+\boldsymbol{C})\boldsymbol{N^2}\left(\sqrt{\boldsymbol{1}+\boldsymbol{\lambda_1}}\cosh\sqrt{\boldsymbol{1}+\boldsymbol{\lambda_1}}\boldsymbol{Nh}+\boldsymbol{N}\beta\sinh\sqrt{\boldsymbol{1}+\boldsymbol{\lambda_1}}\boldsymbol{hN}\right)} \tag{27}$$

$$\boldsymbol{c_4} = -\frac{\sqrt{\boldsymbol{1}+\boldsymbol{\lambda_1}}((-\boldsymbol{1}+\boldsymbol{C})\boldsymbol{E}+\frac{\boldsymbol{dp}}{\boldsymbol{dx}})}{(-\boldsymbol{1}+\boldsymbol{C})\boldsymbol{N}(\sqrt{\boldsymbol{1}+\boldsymbol{\lambda_1}}\cosh\sqrt{\boldsymbol{1}+\boldsymbol{\lambda_1}}\boldsymbol{Nh}+\boldsymbol{N}\beta\sinh\sqrt{\boldsymbol{1}+\boldsymbol{\lambda_1}}\boldsymbol{hN})}, \tag{28}$$

$$\begin{aligned}\boldsymbol{c_5} = {} & \tfrac{1}{8(-1+C)h(1+\lambda_1)^2N^2N_1}(-(-\boldsymbol{1}+\boldsymbol{C})\boldsymbol{c_1^2}\boldsymbol{c_2}\boldsymbol{E_c}\boldsymbol{N_1} - (-\boldsymbol{1}+\boldsymbol{C})\boldsymbol{c_2}\boldsymbol{c_4^2}\boldsymbol{E_c}(\boldsymbol{1}+\boldsymbol{\lambda_1})\boldsymbol{M^2}\boldsymbol{N_1} - \boldsymbol{2}(-\boldsymbol{1}+\boldsymbol{C})\boldsymbol{c_1^2}\boldsymbol{c_2}\boldsymbol{E_c}\boldsymbol{h^2}(\boldsymbol{1}+\boldsymbol{\lambda_1})\boldsymbol{N^2}\boldsymbol{N_1} + \boldsymbol{8}(-\boldsymbol{1}+\boldsymbol{C})(\boldsymbol{1}+\boldsymbol{\lambda_1})^2\boldsymbol{N^2}\boldsymbol{N_1} \\ & +\boldsymbol{2}(-\boldsymbol{1}+\boldsymbol{C})\boldsymbol{c_2}\boldsymbol{c_4^2}\boldsymbol{E_c}\boldsymbol{h^2}(\boldsymbol{1}+\boldsymbol{\lambda_1})^2\boldsymbol{M^2}\boldsymbol{N^2}\boldsymbol{N_1} - \boldsymbol{8}(-\boldsymbol{1}+\boldsymbol{C})\boldsymbol{c_2}\boldsymbol{c_4}(\boldsymbol{1}+\boldsymbol{\lambda_1})\boldsymbol{N_1}(\boldsymbol{2}(\boldsymbol{1}+\boldsymbol{c_3})\boldsymbol{E_c}\boldsymbol{M^2} - \boldsymbol{\Gamma_2}) + \boldsymbol{4}\boldsymbol{c_2}\boldsymbol{h^2}(\boldsymbol{1}+\boldsymbol{\lambda_1})^2\boldsymbol{N^2}((-\boldsymbol{1}+\boldsymbol{C})(\boldsymbol{1}+\boldsymbol{c_3})^2\boldsymbol{E_c}\boldsymbol{M^2}\boldsymbol{N_1} \\ & -\boldsymbol{E_c}(\tfrac{\boldsymbol{dp}}{\boldsymbol{dx}})^2 + (-\boldsymbol{1}+\boldsymbol{C})\boldsymbol{N_1}(\boldsymbol{\Gamma_1}-\boldsymbol{c_3}\boldsymbol{\Gamma_2})) + \boldsymbol{8}(-\boldsymbol{1}+\boldsymbol{C})\boldsymbol{c_2}\boldsymbol{c_4}(\boldsymbol{1}+\boldsymbol{\lambda_1})\boldsymbol{N_1}(\boldsymbol{2}(\boldsymbol{1}+\boldsymbol{c_3})\boldsymbol{E_c}\boldsymbol{M^2}-\boldsymbol{\Gamma_2})\cosh\sqrt{\boldsymbol{1}+\boldsymbol{\lambda_1}}\boldsymbol{Nh} + (-\boldsymbol{1}+\boldsymbol{C})\boldsymbol{c_2}\boldsymbol{E_c}(\boldsymbol{c_1^2} \\ & +\boldsymbol{c_4^2}(\boldsymbol{1}+\boldsymbol{\lambda_1})\boldsymbol{M^2})\boldsymbol{N_1}\cosh\sqrt{\boldsymbol{1}+\boldsymbol{\lambda_1}}\boldsymbol{Nh}),\end{aligned} \tag{29}$$

$$\boldsymbol{c_6} = \frac{\boldsymbol{c_2}((-\boldsymbol{1}+\boldsymbol{C})\boldsymbol{c_1^2}\boldsymbol{E_c}\boldsymbol{N_1} - (-\boldsymbol{1}+\boldsymbol{C})\boldsymbol{c_4^2}\boldsymbol{E_c}(\boldsymbol{1}+\boldsymbol{\lambda_1})\boldsymbol{M^2}\boldsymbol{N_1} - \boldsymbol{2}(\boldsymbol{1}+\boldsymbol{\lambda_1})((-\boldsymbol{1}+\boldsymbol{C})(\boldsymbol{1}+\boldsymbol{c_3})^2\boldsymbol{E_c}\boldsymbol{M^2}\boldsymbol{N_2} - \boldsymbol{E_c}(\tfrac{\boldsymbol{dp}}{\boldsymbol{dx}})^2 + (-\boldsymbol{1}+\boldsymbol{C})\boldsymbol{N_1}(\boldsymbol{\Gamma_1}-\boldsymbol{c_3}\boldsymbol{\Gamma_2})))}{\boldsymbol{4}(-\boldsymbol{1}+\boldsymbol{C})(\boldsymbol{1}+\boldsymbol{\lambda_1})\boldsymbol{N_1}}, \tag{30}$$

The non-dimensional pressure rise Δp is evaluated numerically with the help of computer generated codes by using the following expression:

$$\Delta p = \int_0^1 \frac{dp}{dx}\mathrm{d}x \tag{34}$$

4. Numerical results and discussion

Extensive graphical solutions have been obtained based on computational evaluation of the closed-form solutions presented in Section 3. A parametric study is now conducted of the influence of a number of selected thermo-physical parameters on the peristaltic flow characteristics i.e. fluid and particle phase velocities $(\boldsymbol{u_f}, \boldsymbol{u_p})$, fluid and particle phase temperatures $(\theta_{f,p})$and pressure rise$(\Delta \boldsymbol{p})$. he expression for pressure rise in Eqn. (34) is also evaluated numerically with the help of the symbolic computational software **Mathematica** for the following parametric values: when$\boldsymbol{E_c} = \boldsymbol{0.5}, \boldsymbol{C} = \boldsymbol{0.5}, \boldsymbol{Q} = \boldsymbol{3}, \boldsymbol{P_r} = \boldsymbol{5}, \boldsymbol{\beta} = \boldsymbol{0.2}, \boldsymbol{M} = \boldsymbol{0.4}, \boldsymbol{k} = \boldsymbol{1}, \boldsymbol{R_d} = \boldsymbol{0.5}$. Streamline plots are also presented to visualize bolus formation dynamics in the regime. Table 1 shows the comparison between Newtonian $(\boldsymbol{\lambda_1} = \boldsymbol{0})$ and non-Newtonian fluid $(\boldsymbol{\lambda_1} \neq \boldsymbol{0})$ for velocity and temperature profile.

Please cite this article in press as: M.M. Bhatti et al., Mathematical modelling of nonlinear thermal radiation effects on EMHD peristaltic pumping of viscoelastic dusty fluid through a porous medium duct, Eng. Sci. Tech., Int. J. (2016), http://dx.doi.org/10.1016/j.jestch.2016.11.003

Table 1
Comparison between Newtonian and non-Newtonian fluid for velocity and temperature profile.

Velocity Profile		Temperature profile	
Newtonian	Non-Newtonian	Newtonian	Non-Newtonian
0.93688	1.24213	0	0
0.92582	1.23088	2.83763	1.55248
0.89239	1.19638	5.10913	2.80557
0.83587	1.1364	6.80832	3.75695
0.75504	1.04702	7.92448	4.40224
0.64814	0.92241	8.44183	4.73418
0.51287	0.75447	8.33864	4.74133
0.34630	0.53225	7.58601	4.40598
0.14482	0.24127	6.14639	3.70116
-0.09592	-0.13742	3.97154	2.58618
-0.38114	-0.62850	1	1

4.1. Velocity distributions

Figs. 2–4 illustrate the variation in velocity profile against Hartmann number ($\boldsymbol{M}$), porous media permeability parameter ($\boldsymbol{k}$), particle volume fraction ($\boldsymbol{C}$), Jeffrey fluid parameter (λ_1) and slip parameter (ξ). Fig. 2 that velocity profile decreases due to the increment in the Hartmann number ($\boldsymbol{M}$). When the magnetic field is applied to the fluid, it creates a force transverse to the direction of application of the magnetic field. This body force, known as Lorentz force, $-\boldsymbol{M}^2(\boldsymbol{u_f}+1)$, *which appears only in the fluid phase momentum Eq. (17)*), acts the reverse axial direction and therefore generates resistance which decelerates the flow. The velocity magnitudes are therefore suppressed across the channel. However, when the electric field increases then it boost the fluid velocity very rapidly. Fig. 3 shows that that when the permeability parameter ($\boldsymbol{k}$) increases then the magnitude of the velocity increases. This parameter arises in the Darcian drag force term, $-\frac{1}{\boldsymbol{k}}(\boldsymbol{u_f}+\boldsymbol{1})$, also in the *fluid phase momentum eqn. (17)*. With progressively greater permeability, the matrix resistance offered by the solid fibers in the porous medium is depleted. This suppresses the porous drag force and manifests in a fluid acceleration. Again the velocity magnitudes are significantly lower for the Newtonian fluid compared with the non-Newtonian (viscoelastic) case. Flow acceleration in Jeffreys fluid flows has also been identified in other studies including Gaffar et al. [22]. Fig. 3 indicates that with *greater* particle volume fraction ($\boldsymbol{C}$) the magnitude of the velocity decreases markedly. Hence with increasing presence of solid particles in the dusty suspension, the drag forces are enhanced and flow retardation is induced. These observations also concur with earlier studies and confirm the non-trivial, opposing nature of solid particles present in dusty flows as elaborated by Mekheimer et al. [45],

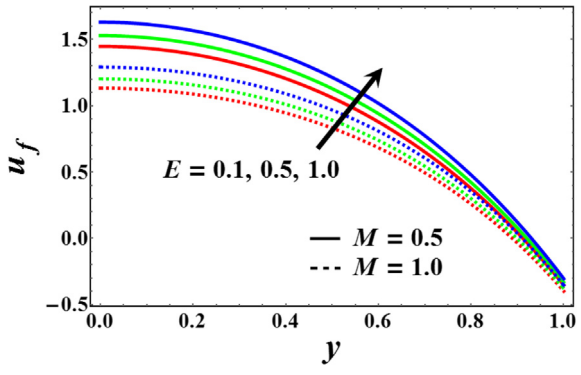

Fig. 2. Velocity evolution across channel semi-width with various values of magnetic body force parameter ($\boldsymbol{M}$) and Electric field ($\boldsymbol{E}$).

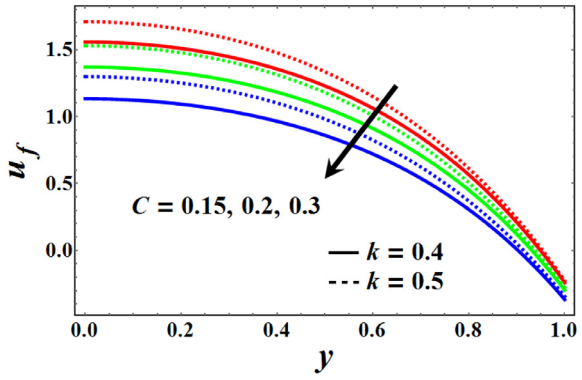

Fig. 3. Velocity evolution across channel with various values of permeability parameter (??) particle volume fraction ($\boldsymbol{C}$).

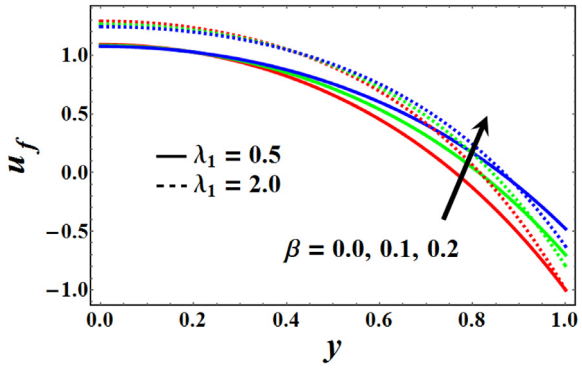

Fig. 4. Velocity profiles for various values of particle volume fraction ($\boldsymbol{C}$) and slip parameter $\boldsymbol{\beta}$.

Bhatti and Zeeshan [46] and Kamel et al. [48]. Further corroboration is documented in Drew [44]. It can be observed from (Fig. 4) when the slip parameter $\boldsymbol{\beta}$ increases then there is a substantial acceleration in the fluid when $y = h$. However, opposite influence has been obtained when $y < 0.3$. In this figure we can also see that when fluid parameter increases then it also enhances the velocity profile. However it is evident that non-Newtonian fluid achieves generally greater velocity than the Newtonian fluid. The relaxation and retardation parameters are both non-zero for the non-Newtonian fluid. These encourage acceleration of the dusty fluid. Moreover, the c by taking $\boldsymbol{\lambda_1 = 0}$.

4.2. Temperature profiles

Figs. 5–7 depict the temperature field (fluid and particle are equivalent, based on the present formulation) response to variation in several key parameters. In Fig. 5, the impact of increasing Prandtl number ($\boldsymbol{P_r}$) is observed to enhance temperatures. This result is important for those fluid which have high Prandtl numbers but less important for those fluids which have very low Prandtl number (ionized gases etc). The Prandtl number is the ratio of momentum diffusivity to the thermal diffusivity. Larger values of Prandtl number correspond to the case of less heat transfer from the boundary to the fluid. Prandtl number is also the product of dynamic viscosity and specific heat capacity divided by the thermal conductivity of the fluid. For $\boldsymbol{P_r} < 1$ *(of relevance to rheological propellants* [49]*)*, thermal diffusivity exceeds the momentum diffusivity and this enhances the transport of heat in the channel dusty suspension, manifesting in an elevation in temperatures. Non-Newtonian (viscoelastic) dusty fluids achieve significantly greater

Please cite this article in press as: M.M. Bhatti et al., Mathematical modelling of nonlinear thermal radiation effects on EMHD peristaltic pumping of viscoelastic dusty fluid through a porous medium duct, Eng. Sci. Tech., Int. J. (2016), http://dx.doi.org/10.1016/j.jestch.2016.11.003

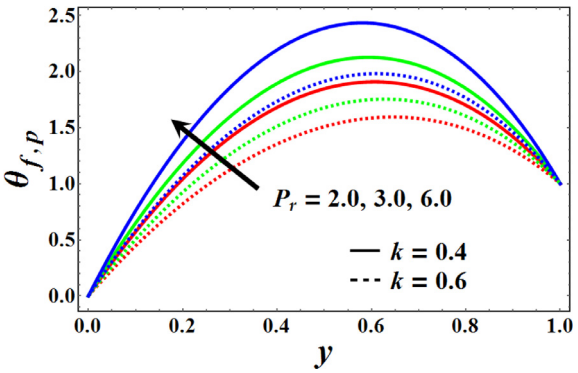

Fig. 5. Temperature profiles for various values of Prandtl number (**Pr**) and permeability parameter (***k***).

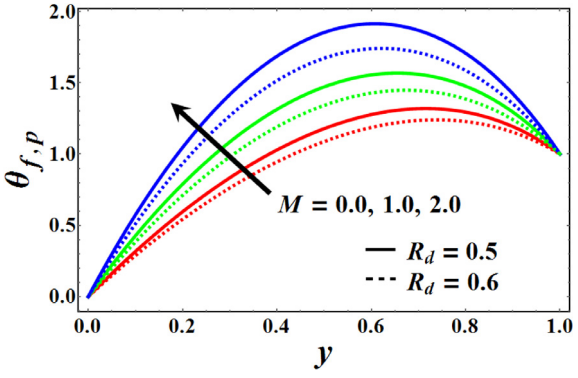

Fig. 6. Temperature profiles for various values of radiation-conduction number ($\boldsymbol{R_d}$) and magnetic parameter (***M***).

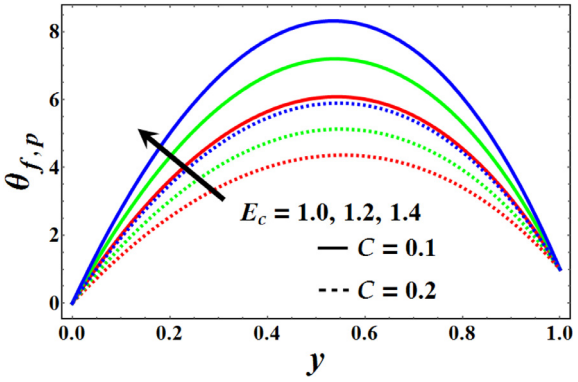

Fig. 7. Temperature profiles for various values of Eckert number (***Ec***) and particle volume fraction (***C***).

temperatures than Newtonian fluids, as also observed by Kamel et al. [48]. Fig. 5 shows that with an increment in the permeability parameter (***k***), there is a reduction in temperature profiles. The parameter k is directly proportional to the permeability of the porous medium in the channel. Since the medium is isotropic only a single permeability is required. As *k* increases, the concentration of solid fibers is reduced and this suppresses thermal conduction heat transfer. This leads to a decrease in temperatures i.e. cooling of the regime. Fig. 6 demonstrates that with larger values of radiation parameter ($\boldsymbol{R_d} = \frac{4\sigma T^3}{k\mu_s c(1-C)}$),the temperature profiles for *both* the fluid and particle phase decrease. As ($\boldsymbol{R_d}$) increases the transport by electromagnetic waves is enhanced whereas that due to thermal conduction is suppressed. The latter has a profound influence on thermal diffusion in the regime. Since diffusion heat transfer is due to random molecular motion, when this is quenched, neighbouring molecules move less vigorously and transfer energy less efficiently between one another. The time scale for radiative heat transfer is much smaller than diffusive heat transfer. The impact is to cool the regime and decrease temperatures, as observed in Fig. 7. The response for dusty (multi-phase) fluids is therefore the opposite to that for *single phase* fluids, as described in Yang et al. [1] and Srinivas and Muthuraj [15], where for the latter thermal radiation flux generally enhances temperatures. Fig. 6 clearly reveals that with increasing magnetic field parameter (*M*), temperature profile increases. The supplementary work expended in dragging the dusty fluid against the action of the inhibiting magnetic field, is dissipated as *thermal energy*. This energizes the dusty suspension and elevates temperatures. This is a classical observation in magneto-hydrodynamics and plasma dynamics (see Cramer and Pai [50]) and is achieved for both Newtonian and non-Newtonian fluids. The implication for designers is that more efficient heat transfer is attained with non-Newtonian working dusty fluids than Newtonian dusty fluids, and this tends to be in concurrence with the experimental observations of Florczak et al. [49]. Fig. 7 depicts the response in temperature to a change in the Eckert number ($\boldsymbol{E_c}$). Temperature profile significantly increases with greater Eckert number ($\boldsymbol{E_c}$). This parameter represents the conversion of kinetic energy in the channel flow to heat via viscous dissipation. The addition of this supplementary heat significantly elevates temperatures. The values analysed are appropriate for viscous, incompressible flows. Higher values ($\boldsymbol{E_c} > 2$) are associated with compressible flows and are not relevant to the current inves-

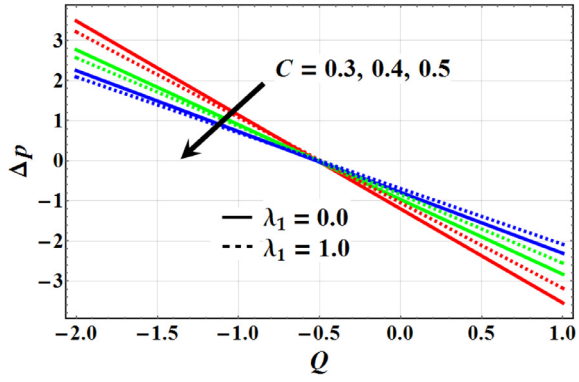

Fig. 8. Pressure rise *vs* volume flow rate for various values of particle volume fraction (***C***) and Jeffrey fluid parameter ($\boldsymbol{\lambda_1}$).

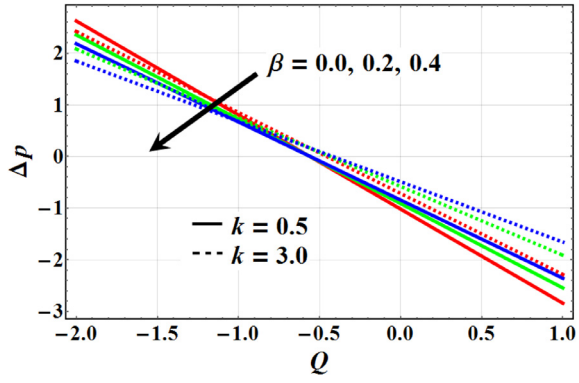

Fig. 9. Pressure rise *vs* volume flow rate for various values of permeability parameter (***k***) and slip parameter ($\boldsymbol{\beta}$).

Please cite this article in press as: M.M. Bhatti et al., Mathematical modelling of nonlinear thermal radiation effects on EMHD peristaltic pumping of viscoelastic dusty fluid through a porous medium duct, Eng. Sci. Tech., Int. J. (2016), http://dx.doi.org/10.1016/j.jestch.2016.11.003

tigation. Inspection of Fig. 7 demonstrates that when the particle volume fraction increases then temperature profile decreases. The presence of solid particles in the dusty fluid therefore consistently depresses the thermal efficiency of transport in the channel. Particles may therefore be introduced judiciously to regulate excessively high temperatures during propulsion.

4.3. Pumping characteristics

(Figs. 8–10) illustrate the pumping characteristics of the propulsion system via plots of pressure rise versus volumetric flow rate.

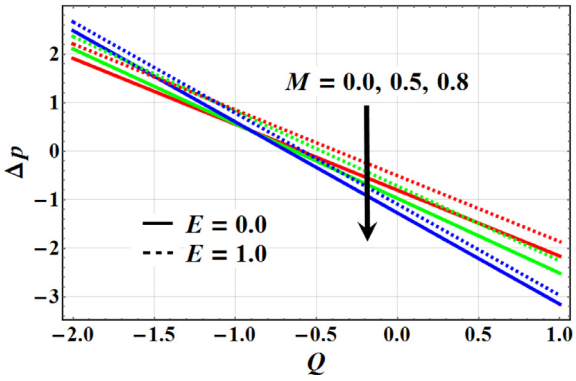

Fig. 10. Pressure rise *vs* volume flow rate for various values of magnetic parameter (***M***) and Electric field (*E*).

Fig. 8 shows that when the particle volume fraction (***C***)increases then the pumping rate decreases in *the retrograde pumping region* whereas the converse response (i.e. an increase) is computed in the *co-pumping region*. From Fig. 9 it is apparent that when the permeability parameter (***k***) increases, in the *retrograde pumping region* the *pumping rate decreases; however* in the co-pumping region the opposite behaviour is induced and pumping rate strongly *increases*. It can analyse from Fig. 8 that with the increment in slip parameter (***β***), pumping rate decreases in retrograde pumping region, but its behavior is adverse in free pumping region and co-pumping region. Fig. 10 shows that with greater Hartmann (magnetic body force) number (***M***) the pumping rate *increases* in the retrograde pumping region and when volume flow rate (***Q***) increases then reverse flow occurs which diminishes the pumping rate in co-pumping region. It depicts from Fig. 10 that the impact of electric field shows similar behavior in all the regions but in the presence of electric field ($E \neq 0$) the pressure increases.

4.4. 4Trapping mechanism

Another key hydrodynamic characteristic of peristaltic propulsion is *trapping*, which is visualized best via drawing contours. It generally represents the formation of internally circulating bolus in the fluid. The volume of the bolus in the fluid is enclosed by the stream lines. For this purpose, (Figs. 11–15) are sketched against Hartmann number, particle volume fraction, slip parameter, electric field and permeability parameter. The expression for dimensionless stream function satisfying the D'Alembert continuity equation is defined as:

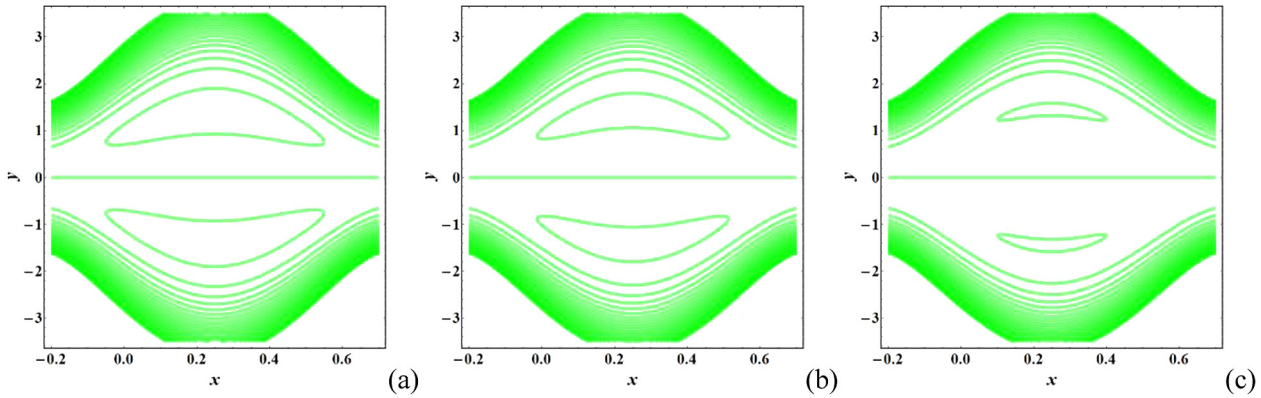

Fig. 11. Contour plots for various values of magnetic parameter (***M***) : (**a**)$\boldsymbol{M} = \mathbf{0}$, (***b***)$\boldsymbol{M} = \mathbf{0.4}$, (***c***)$\boldsymbol{M} = \mathbf{0.6}$.

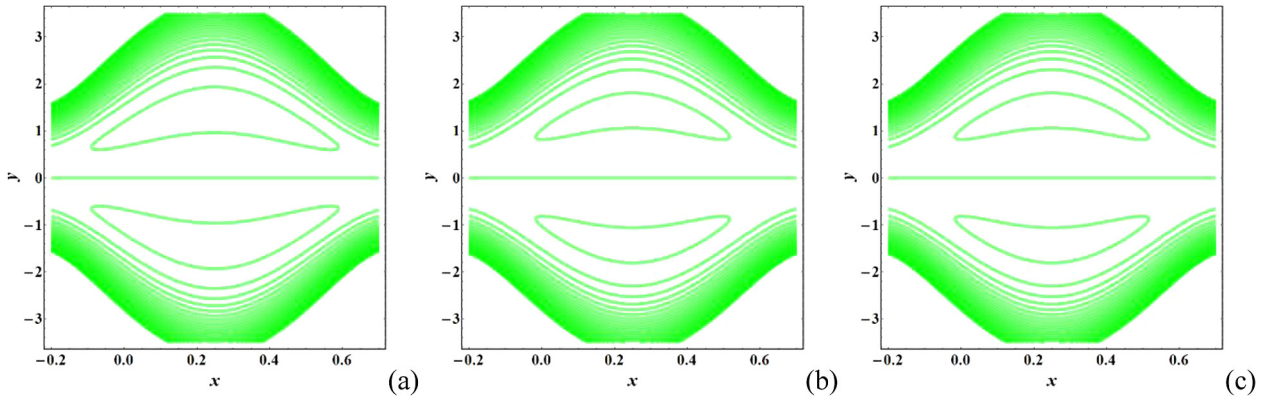

Fig. 12. Contour plots for various values of particle volume fraction (***C***): (**a**)$\boldsymbol{C} = \mathbf{0.1}$, (***b***)$\boldsymbol{C} = \mathbf{0.15}$, (***c***)$\boldsymbol{C} = \mathbf{0.2}$.

Please cite this article in press as: M.M. Bhatti et al., Mathematical modelling of nonlinear thermal radiation effects on EMHD peristaltic pumping of viscoelastic dusty fluid through a porous medium duct, Eng. Sci. Tech., Int. J. (2016), http://dx.doi.org/10.1016/j.jestch.2016.11.003

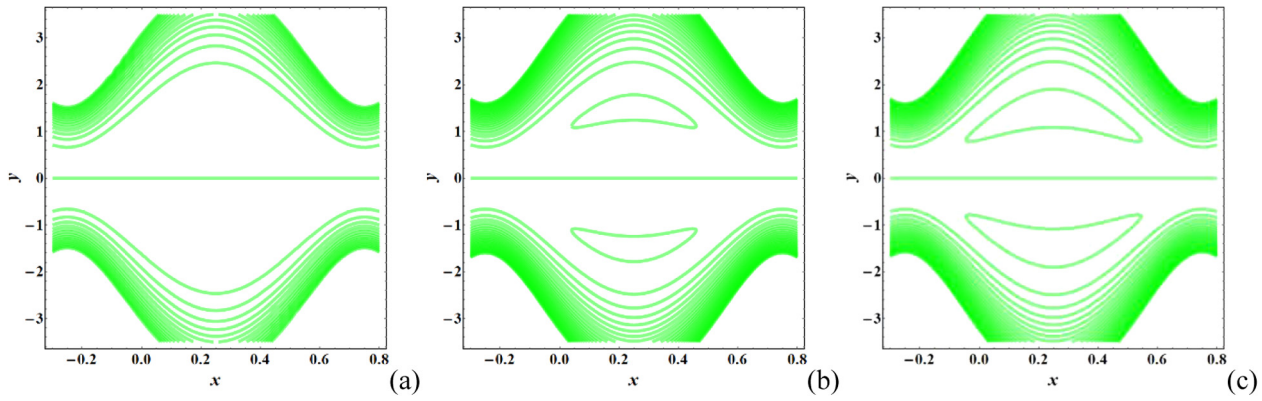

Fig. 13. Contour plots for various values of permeability parameter (k) (**a**)$C = 0.1$, (**b**)$C = 0.15$, (**c**)$C = 0.2$.

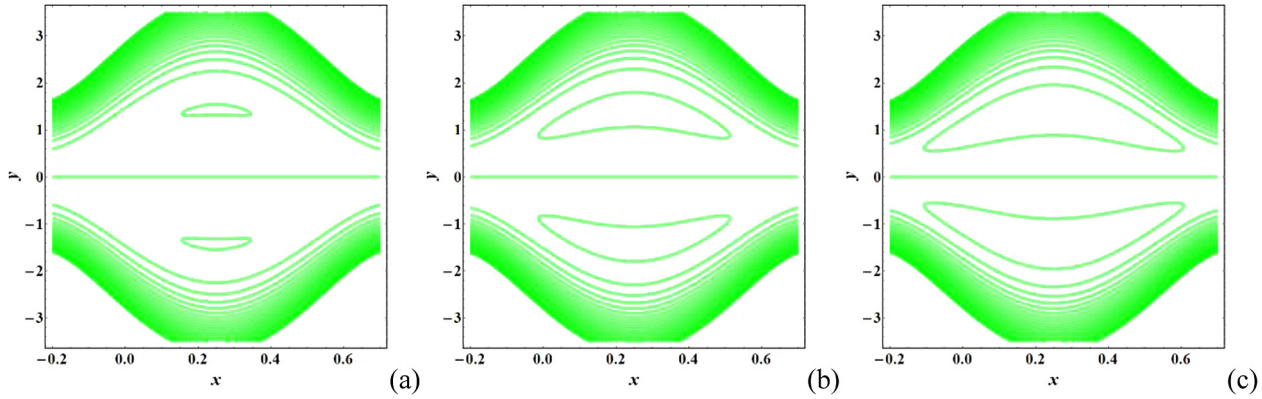

Fig. 14. Contour plots for various values of slip parameter (β) (**a**)$\beta = 0.1$, (**b**)$\beta = 0.2$, (**c**)$\beta = 0.5$.

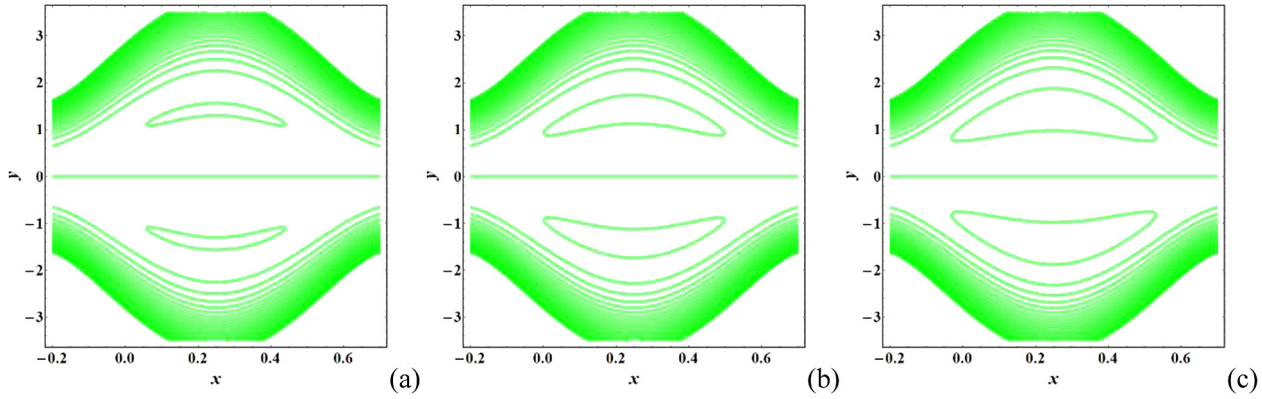

Fig. 15. Contour plots for various values of Electric field (E) (**a**)$E = 0.0$, (**b**)$E = 0.3$, (**c**)$E = 0.8$.

$$u_{f,p} = \frac{\partial \varphi_{f,p}}{\partial y}, \quad v_{f,p} = -\frac{\partial \varphi_{f,p}}{\partial x} \tag{35}$$

Fig. 11 demonstrates that when the Hartmann number (M) increases then the *size* of the trapping bolus decreases very rapidly whereas the *number* of trapping boluses remains same. It is also evident from Fig. 12 that the impact of *increasing particle volume fraction* (i.e. greater concentration of solid particles in the dusty suspension) is to reduce the magnitude of the trapping bolus whereas it does not cause any major effect on the *number of trapped boluses*. Fig. 13 shows that with greater permeability (k) i.e. increased hydrodynamic transmissivity of the porous medium to percolating dusty suspension flow, the size of the bolus is modified very slowly, whereas, the number of the bolus are constant. It can examined from Fig. 14 that for large values of slip parameter (β) the magnitude of the trapped bolus increases significantly. Fig. 15 shows that effects of electric field on trapping phenomena. As, we can see from this figure that for large values of electric field (E), a trapping bolus has been observed and it grows in size for higher values of electric field (E).

Additionally we note that it is possible to extend the present analysis to include other characteristics e.g. velocity gradient (shear stress), temperature gradient (Nusselt number) etc which can be evaluated from derivatives of the fundamental functions (velocity and temperature) which have already been studied. For brevity these have been omitted.

Please cite this article in press as: M.M. Bhatti et al., Mathematical modelling of nonlinear thermal radiation effects on EMHD peristaltic pumping of viscoelastic dusty fluid through a porous medium duct, Eng. Sci. Tech., Int. J. (2016), http://dx.doi.org/10.1016/j.jestch.2016.11.003

5. Conclusions

A mathematical model has been developed for the influence of nonlinear thermal radiation on Electromagnetohydrodynamic (EMHD) dissipative flow and heat transfer in a viscoelastic, electro-conductive, dusty (fluid-particle) suspension through a uniform porous medium planar channel. Analytical solutions have been derived for the transformed, dimensionless conservation equations for the fluid and particulate phase, subject to physically viable boundary conditions at the channel walls. The major outcomes of the present analysis are summarized below:

- Velocity of the fluid is enhanced with increasing permeability of the porous medium whereas the converse behaviour is computed with increasing Hartmann (magnetic field) parameter and particle volume fraction.
- With increasing Prandtl number and Eckert number, temperatures are significantly elevated.
- Increasing thermal radiation flux (and decreasing conduction heat transfer contribution) and increasing permeability are observed to suppress temperatures in the channel.
- Both fluid velocity and fluid and particle temperatures are markedly reduced with an increase in particle volume fraction.
- With an increment in slip parameter parameter there is an associated elevation in velocity profile.
- Pressure rise is strongly modified with a change in the particle volume fraction and permeability parameters.
- Increasing Hartmann (magnetic) number reduces the *size* of the trapping bolus but the quantity of these boluses are constant.
- Increasing particle volume fraction (i.e. higher concentration of solid particles in the dusty suspension) decreases the size of the trapping bolus very slowly.
- Increasing greater the size of the bolus is modified weakly and there is no change in the quantity of trapping boluses.

The present study has revealed some important characteristics of non-Newtonian dusty flow and heat transfer in magnetized peristaltic propulsion systems. However other rheological models exist which may further elucidate mechanisms of momentum and heat transfer e.g. micropolar fluids [24], and these will be addressed in the near future. Two-phase nanofluids also present significant potential for propulsion thermofluid dynamics and interesting studies using these models include Dinarvand et al. [51,52]. Furthermore more complex radiative transfer models (e.g. P1 differential model) [3] may be employed to simulate moment intensity characteristics in the dusty suspension. The subject provides a rich arena for mathematical simulation and it is also hoped that the present investigation will further stimulate experimental studies of magnetic propulsion and heat transfer in non-Newtonian fluids.

References

[1] G. Yang, M.A. Ebadian, A. Campo, Radiation convection in a thermally developing duct flow of noncircular cross section, AIAA J. Thermophys. Heat Transfer 5 (1991) 224–231.
[2] G.H. Watson, A.L. Lee, Thermal radiation model for solid rocket booster plumes, AIAA J. Spacecraft Rockets 14 (11) (1977) 641–647.
[3] O. Anwar Bég, N. Ali, A. Zaman, A. Eemaan, T.A. Bég, Ayesha Sohail, Computational modelling of heat transfer in annular porous medium solar energy absorber with a P1-radiative differential approximation, J. Taiwan Inst. Chem. Eng. (2016), http://dx.doi.org/10.1016/ j.jtice.2016.06.034 (11 pages).
[4] V. Rajesh, O. Anwar Bég, M.P. Mallesh, Transient nanofluid flow and heat transfer from a moving vertical cylinder in the presence of thermal radiation. Numerical study, Proc. IMECHE- Part N. J. Nanoeng. Nanosyst. 230 (2016) 3–16.
[5] B. Marracino, D. Lentini, Radiation modelling in non-premixed turbulent flames, Combust. Sci. Technol. 128 (1997) 23–48.
[6] N. Takahashi, H. Koseki, T. Hirano, Temporal and spatial characteristics of radiation from large pool fires, Bull. Jpn. Assoc. Fire Sci. Eng. 49 (1) (1999) 27–33.
[7] A. Ogulu, J. Prakash, Heat transfer to unsteady magneto-hydrodynamic flow past an infinite moving vertical plate with variable suction, Phys. Scr. 74 (2006) 232–239.
[8] M.J. Uddin, O. Anwar Bég, A.I. Ismail, Radiative-convective nanofluid flow past a stretching/shrinking sheet with slip effects, AIAA J. Thermophys. Heat Transfer 29 (3) (2015) 513–523.
[9] S. Murthy, A.G. Fedorov, Radiation heat transfer analysis of the monolith-type solid oxide fuel cell, J. Power Sources 124 (2) (2003) 453–458.
[10] F. Göbel, C. Mundt. Implementation of the P1 radiation model in the CFD solver NSMB and investigation of radiative heat transfer in the SSME main combustion chamber, in: 17th AIAA International Space Planes and Hypersonic Systems and Technologies Conference, International Space Planes and Hypersonic Systems and Technologies Conferences, San Francisco, California, USA. April, 2011.
[11] O. Anwar Bég, M.J. Uddin, M.M. Rashidi, N. Kavyani, Double-diffusive radiative magnetic mixed convective slip flow with Biot and Richardson number effects, J. Eng. Thermophys. 23 (2) (2014) 79–97.
[12] R. Siegel, J.R. Howell, Thermal Radiation Heat Transfer, Prentice-Hall, USA, 1972.
[13] M.M. Rahman, I.A. Eltayeb, Radiative heat transfer in a hydromagnetic nanofluid past a non-linear stretching surface with convective boundary condition, Meccanica 48 (2013) 601–615.
[14] O. Anwar Bég, S.K. Ghosh, M. Narahari, T.A. Bég, Mathematical modelling of thermal radiation effects on transient gravity-driven optically-thick gray convection flow along an inclined plate with pressure gradient, Chem. Eng. Commun. 198 (2011) 1–15.
[15] S. Srinivas, R. Muthuraj, Effects of thermal radiation and space porosity on MHD mixed convection flow in a vertical channel using homotopy analysis method, Commun. Nonlinear Sci. Numer. Simul. 15 (2010) 2098–2108.
[16] M. Ferdows, M.S. Khan, O. Anwar Bég, M.A.K. Azad, M.M. Alam, Numerical study of transient magnetohydrodynamic radiative free convection nanofluid flow from a stretching permeable surface, Proc. IMechE-Part E: J. Process. Mech. Eng. 228 (3) (2014) 181–196.
[17] A. Zeeshan, A. Majeed, R. Ellahi, Effect of magnetic dipole on viscous ferro-fluid past a stretching surface with thermal radiation, J. Mol. Liq. 215 (2016) 549–554.
[18] O. Anwar Bég, M. Ferdows, Bég A. Tasveer, T. Ahmed, M. Wahiduzzaman, Md. M. Alam, Radiative optically-dense magnetized transient reactive transport phenomena with cross diffusion and dissipation effects, Numer. Simul. J. Taiwan Inst. Chem. Eng. (2016) 15, http://dx.doi.org/10.1016/J.JTICE.2016.06.003.
[19] S. Snyder, N. Arockiam, P.E. Sojka, Secondary Atomization of elastic non-Newtonian liquid drops, in: AIAA Joint Propulsion Conference, Nashville, Tennessee, USA, June, 2010.
[20] O. Anwar Bég, S.S. Motsa, M.N. Islam, M. Lockwood, Pseudo-spectral and variational iteration simulation of exothermically-reacting Rivlin-Ericksen viscoelastic flow and heat transfer in a rocket propulsion duct, Comput. Therm. Sci. 6 (2014) 91–102.
[21] F. Irgens, Rheology and Non-Newtonian Fluids, Springer, Germany, 2014.
[22] S. Abdul Gaffar, V.R. Prasad, O. Anwar Bég, Flow and heat transfer of Jeffreys non-Newtonian fluid from a horizontal circular cylinder, AIAA J. Thermophys. Heat Transfer 28 (2014) 764–770.
[23] M.S. Abel, N. Mahesha, Heat transfer in MHD viscoelastic fluid flow over a stretching sheet with variable thermal conductivity. non-uniform heat source and radiation, Appl. Math. Model. 32 (2008) 1965–1983.
[24] D. Gupta, Lokendra Kumar, O. Anwar Bég, Bani Singh, Finite element simulation of mixed convection flow of micropolar fluid over a shrinking sheet with thermal radiation, Proc. IMech. E- Part E: J. Process Mech. Eng. 228 (1) (2014) 61–72.
[25] M. Khan, R. Malik, M. Hussain, Nonlinear radiative heat transfer to stagnation-point flow of Sisko fluid past a stretching cylinder, AIP Adv. 6 (2016) 055315, http://dx.doi.org/10.1063/1.4950946.
[26] M.J. Uddin, O. Anwar Bég, P.K. Ghose, A.I.M. Ismael, Numerical study of non-Newtonian nanofluid transport in a porous medium with multiple convective boundary conditions and nonlinear thermal radiation effects, Int. J. Num. Meth. Heat Fluid Flow 26 (5) (2016) 1–25, http://dx.doi.org/10.1108/HFF-03-2015-0123.
[27] M. Mustafa, Rida Ahmad, T. Hayat, A. Alsaedi, Rotating flow of viscoelastic fluid with nonlinear thermal radiation: a numerical study, Neural Comput. Appl. (2016) 7, http://dx.doi.org/10.1007/s00521-016-2462-x.
[28] A. Subba Rao, V.R. Prasad, K. Harshavalli, O. Anwar Bég, Thermal radiation effects on non-Newtonian fluid in a variable porosity regime with partial slip. J. Porous Media, 19 (4), 1–17.
[29] Y.C. Fung, Biomechanics: Motion, Flow, Stress and Growth, Springer, New York, 1990.
[30] Y. Bar-cohen, Z. Chatig, Piezoelectrically-Actuated Miniature Peristaltic Pump, Caltech- Jet Propulsion Laboratory, Technical Report, Pasadena, California, USA, 1991.
[31] V. Shkolnikov, J. Ramunas, J.G. Santiago, A self-priming, roller-free, miniature, peristaltic pump operable with a single, reciprocating actuator, Sens. Actuators, A Phys. 160 (1–2) (2010) 141–146.
[32] J. Slough, A. Blair, C. Pihl, G. Votroubek, Magnetically accelerated plasmoid (MAP) thruster – initial results and future plans. IEPC paper 2007–16, in: 30th Int. Electric Propulsion Conference, Florence, Italy, September 17–20, 2007.
[33] D. Kim et al., Quantitative analysis of pneumatically driven biomimetic micro peristalsis, Sci. Adv. Mater. 6 (11) (2014) 2428–2434.

Please cite this article in press as: M.M. Bhatti et al., Mathematical modelling of nonlinear thermal radiation effects on EMHD peristaltic pumping of viscoelastic dusty fluid through a porous medium duct, Eng. Sci. Tech., Int. J. (2016), http://dx.doi.org/10.1016/j.jestch.2016.11.003

[34] T. Hayat, M.U. Qureshi, Q. Hussain, Effect of heat transfer on the peristaltic flow of an electrically conducting fluid in a porous space, Appl. Math. Model. 33 (2009) 1862–1873.
[35] D. Tripathi, O. Anwar Bég, A study of unsteady physiological magneto-fluid flow and heat transfer through a finite length channel by peristaltic pumping, Proc. IMechE Part H-J. Eng. Med. 226 (2012) 631–644.
[36] S. Srinivas, M. Kothandapani, The influence of heat and mass transfer on MHD peristaltic flow through a porous space with compliant walls, Appl. Math. Comput. 213 (2009) 197–208.
[37] S.K. Pandey, M.K. Chaube, Peristaltic flow of a micropolar fluid through a porous medium in the presence of an external magnetic field, Commun. Nonlinear Sci. Numer. Simul. 16 (2011) 3591–3601.
[38] O. Anwar Bég, M.M. Rashidi, Multi-Step DTM simulation of magneto-peristaltic flow of a conducting Williamson viscoelastic fluid, Int. J. Appl. Math. Mech. 9 (12) (2013) 22–40.
[39] T. Hayat, Z. Nisar, B. Ahmad, H. Yasmin, Simultaneous effects of slip and wall properties on MHD peristaltic motion of nanofluid with Joule heating, J. Mag. Mag. Mater. 395 (2015) 48–58.
[40] N.S. Akbar, D. Tripathi, O. Anwar Bég, Modelling nanoparticle geometry effects on peristaltic pumping of medical magnetohydrodynamic nanofluids with heat transfer, J. Mech. Med. Biol. 16 (2) (2016) 1650088.1–1650088.20.
[41] A.A. Khan, R. Ellahi, M. Usman, The effects of variable viscosity on the peristaltic flow of non-Newtonian fluid through a porous medium in an inclined channel with slip boundary conditions, J. Porous Media 16 (2013) 59–67.
[42] D. Tripathi, O. Anwar Bég, P.K. Gupta, G. Radhakrishnamacharya, J. Mazumdar, DTM simulation of peristaltic viscoelastic biofluid flow in asymmetric porous media: a digestive transport model, J. Bionic Eng. 12 (4) (2015) 1–13.
[43] O.U. Mehmood, C. Fetecau, A note on radiative heat transfer to peristaltic flow of Sisko fluid, Appl. Bionics Biomech. 2015 (2015) 9, http://dx.doi.org/10.1155/2015/283892. Article ID 283892.
[44] D.A. Drew, Mathematical modeling of two-phase flow, Annu. Rev. Fluid Mech. 15 (1983) 261–291.
[45] K.S. Mekheimer, E.F.E.L. Shehawey, A.M. Elaw, Peristaltic motion of a particle-fluid suspension in a planar channel, Int. J. Theor. Phys. 37 (1998) 2895–2920.
[46] M.M. Bhatti, A. Zeeshan, Heat and mass transfer analysis on peristaltic flow of particle–fluid suspension with slip effects, J. Mech. Med. Biol. (2016), http://dx.doi.org/10.1142/S0219519417500282.
[47] P. Nagarani, G. Sarojamm, Peristaltic transport of small particles - power law fluid suspension in a channel, Aust. Phys. Eng. Sci. Med. 30 (2007) 185–190.
[48] M.H. Kamel, I.M. Eldesoky, B.M. Maher, R.M. Abumandour, Slip effects on peristaltic transport of a particle-fluid suspension in a planar channel, Appl. Bionics Biomechan. 2015 (2015) 14. Article ID 703574.
[49] B. Florczak, E. Bednarczyk, A. Maranda, Studies of rheological properties of suspension of heterogeneous rocket propellant based on HTPB rubber, Chemik 69 (3) (2015) 136–145.
[50] K.C. Cramer, S.I. Pai, Applied Magnetofluid Dynamics for Engineers and Applied Physicists, MacGraw-Hill, New York, 1973.
[51] Saeed Dinarvand, Reza Hosseini, Milad Abulhasansari, Ioan Pop, Buongiorno's model for double-diffusive mixed convective stagnation-point flow of a nanofluid considering diffusiophoresis effect of binary base fluid, Adv. Powder Technol. 26 (2015) 1423–1434.
[52] Saeed Dinarvand, Reza Hosseini, Ioan Pop, Unsteady convective heat and mass transfer of a nanofluid in Howarth's stagnation point by Buongiorno's model, Int. J. Numer. Meth. Heat Fluid Flow 25 (5) (2015) 1176–1197.

Please cite this article in press as: M.M. Bhatti et al., Mathematical modelling of nonlinear thermal radiation effects on EMHD peristaltic pumping of viscoelastic dusty fluid through a porous medium duct, Eng. Sci. Tech., Int. J. (2016), http://dx.doi.org/10.1016/j.jestch.2016.11.003